BJR https://doi.org/10.1259/bjr.20230240

Received: 13 March 2023 | Accepted: 25 July 2023 | Published online: 26 September 2023

Cite this article as:
Castagnoli F, Donners R, Tunariu N, Messiou C, Koh D-M. Relative fat fraction of malignant bone lesions from breast cancer, prostate cancer and myeloma are significantly lower than normal bone marrow and shows excellent interobserver agreement. *Br J Radiol* (2023) 10.1259/bjr.20230240.

FULL PAPER

Relative fat fraction of malignant bone lesions from breast cancer, prostate cancer and myeloma are significantly lower than normal bone marrow and shows excellent interobserver agreement

[1,2]FRANCESCA CASTAGNOLI, MD, [1]RICARDO DONNERS, MD, [1,2]NINA TUNARIU, MD, FRCR, MRCP, MDRes, MBBS, [1,2]CHRISTINA MESSIOU, MD, BMed Sci, BMBS, MRCP, FRCR and [1,2]DOW-MU KOH, MD, MRCP, FRCR

[1]Department of Radiology, Royal Marsden Hospital, Sutton, UK
[2]Division of Radiotherapy and Imaging, The Institute of Cancer Research, Sutton, UK

Address correspondence to: Dr Francesca Castagnoli
E-mail: *francesca.castagnoli@rmh.nhs.uk*

Objectives To compare relative fat fraction (rFF) of active bone lesions from breast, prostate and myeloma malignancies and normal bone marrow; to assess its inter-reader agreement.

Methods Patients with breast (n = 26), myeloma (n = 32) and prostate cancer (n = 52) were retrospectively evaluated. 110 baseline rFF maps from whole-body MRI were reviewed by two radiologists. Regions of interest for up to four focal active lesions in each patient were drawn on rFF maps, one each at the cervicothoracic spine, lumbosacral spine, pelvis and extremity. The mean and standard deviation of rFF were recorded. The rFF of normal marrow was measured in the pelvis for patients without diffuse bone disease (n = 88). We compared the rFF of malignant bone lesions and normal marrow using Mann–Whitney test. Interobserver agreement was assessed by interclass correlation coefficient.

Results Malignant bone lesions showed significantly lower median rFF (13.87%) compared with normal marrow (89.76%) with little overlap ($p < 0.0001$). There was no significant difference in the median rFF of malignant lesions from breast (14.46%), myeloma (13.12%) and prostate cancer (13.67%) ($p > 0.017$, Bonferroni correction) and in the median rFF of bone disease according to their anatomical locations ($p > 0.008$, Bonferroni correction). There was excellent interobserver agreement (0.95).

Conclusion The low rFF of active bone lesions in breast, prostate and myeloma malignancies provides high image contrast relative to normal marrow that may be used to detect bone metastases.

Advances in knowledge This study shows the importance of rFF towards detecting bone metastases.

INTRODUCTION

Bone disease is common in advanced cancers; previous studies have shown that the prevalence of bone metastases is more than 70% in patients with breast and prostate cancer.[1,2] In addition, multiple myeloma (MM) can also result in focal lesions within the bone marrow of the axial and appendicular skeletons. Whole body MRI (WB-MRI) has emerged as the most sensitive technique for detecting focal lesions within the bone marrow.[3] In oncological patients, accurate detection and staging of bone disease burden are essential to plan effective treatment.

Gradient-echo-based Dixon T_1 weighted MRI is now frequently employed in WB-MRI protocols.[3,4] Dixon T_1 weighted MRI enables rapid acquisition of T_1 weighted anatomical images to collaborate with the diffusion-weighted imaging for disease assessment. The Dixon technique provides T_1 weighted in-phase, opposed or out-of-phase, fat- and water-only images within a single acquisition. The fat- and water-only images can be used to calculate the relative fat-fraction (rFF) maps, which provide additional insights into bone disease status.[5,6] In myeloma, response of bone disease to treatment has been shown to increase the rFF of involved bone marrow and an early

Figure 1. rFF map of a 51-year-old patient with breast cancer. A metastatic lesion is seen in the left pedicle of T11 (arrow) which is characterised by low signal intensity on rFF map compared with normal fat-containing bone marrow (*). rFF, relative fat fraction.

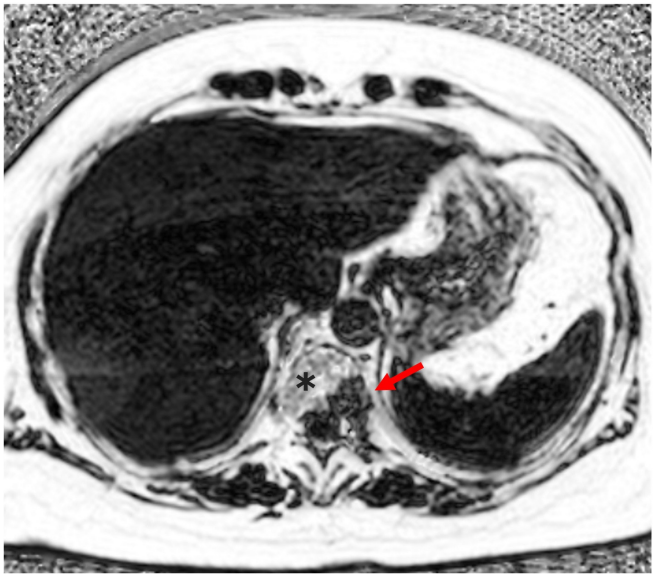

increase in lesional rFF has also been shown to be associated with response to chemotherapy.[7]

As metastases and malignant bone disease do not usually contain fat, malignant bone disease is expected to show significant lower rFF compared with normal fat-containing bone marrow (Figure 1). However, there has been a paucity of studies assessing the differences in the percentage of rFF between normal bone marrow and bone disease. Furthermore, it is unclear whether malignant bone disease arising from different primary tumours have differences in their rFF values. Hence, the aim of this study is to compare the rFF of active bone lesions arising from breast, prostate and myeloma malignancies, and also with the rFF of normal bone marrow. Additionally, we aim to establish the inter-reader agreement of rFF measurements.

METHODS AND MATERIALS

Study population

This retrospective study was approved by our institutional review board. The requirement for written informed consent was waived.

The patient inclusion criteria were as follows: (1) histologically proven myeloma, breast or prostate cancer, (2) underwent baseline WB-MRI within 30 days of the initiating treatment or a change in therapy; (3) at least one site of bone disease demonstrated on imaging; (4) no other significant intercurrent medical illness. Database search of patients in our hospital (between January 2019 and December 2019) was performed.

Whole-body MRI (WB-MRI) studies

WB-MRI studies were performed using Avanto and Aera 1.5 T systems (Siemens Healthineers). All subjects were scanned supine with arms by their sides. Anterior receiver coil elements were positioned from the skull vertex to the knees. Currently used WB-MRI protocol is summarised in Table 1. The rFF maps were calculated by (fat-only image)/(fat-only image+water-only image) x 100%. No intravenous gadolinium contrast was administered. The typical duration of our WB-MRI examination was 45 min.

Image analysis

The rFF maps were used to select up to four active bone lesions that appeared as low signal intensity areas on the rFF map, show impeded diffusion on the b900 DWI and returned ADC values in the range of 500–1500 mm^2/s. Image analysis was performed in each patient by two radiologists, both with 6 years of experience of MRI reporting. All measurements were performed on a PACS workstation (Sectra, IDS7, v. XX). To ensure that the same lesions were assessed by both readers, the lesions in any part of the imaged volume were selected and analysed by the first reader, who marked them on PACS (Figure 2). Subsequently, the second reader measured the rFF values on the selected lesions.

Each target lesion was chosen at different imaging stations in the body, one each at the cervicothoracic spine, lumbosacral spine, pelvis and extremity. For each lesion, a single region of interest

Table 1. Whole-body MRI protocol

Sequence	Protocol
Sagittal T_1 weighted images	TR 590 ms, TE 11 ms, FOV 400 mm, slice thickness 4 mm
Sagittal T_2 weighted images	TR 2690 ms, TE 93 ms, FOV 400 mm, slice thickness 4 mm
Axial diffusion-weighted sequences	Single-shot double spin-echo echoplanar technique with STIR fat suppression in free breathing Three b values (50, 600 and 900 s/mm^2); highest b value multiplanar reformats and 3D maximum intensity projection reconstructions 40 slices per station (slice thickness 5 mm, no gap, FOV 430 mm, phase direction AP, parallel imaging (GRAPPA) factor 2, TR 14800 ms, TE 66 ms, TI 180 ms, voxel size 2.9 × 2.9 × 5 mm, number of signal averages 4, matrix 150 × 150, bandwidth 1960 Hz per pixel)
Axial T_1 weighted Vibe Dixon 3D gradient echo breath-hold	FOV 470 mm, TR/TE 7/2.38, 4.76 ms, flip angle 30, matrix 192 × 192

3D, three-dimensional; FOV, field of view; STIR, short tau inversion recovery; TE, echo time; TI, inversion time; TR, repetition time.

Figure 2. Regions of interest drawn on rFF maps in patients with prostate (a), myeloma (b) and breast cancer (c). The lesions appear as low signal intensity areas on the rFF map (arrows), whereas normal bone marrow appears as high signal intensity areas (*). rFF, relative fat fraction.

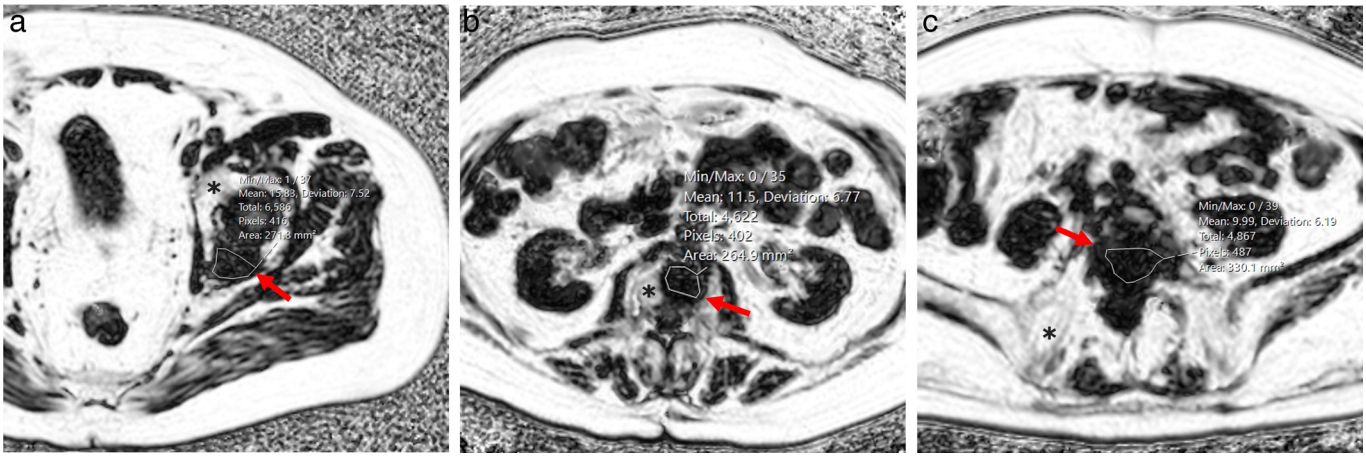

(ROI) was manually drawn within each selected lesion on the rFF maps. The mean (FF-Mean) and standard deviation (FF-SD) of the voxel values within each ROI were recorded, together with the ROI area (FF-Area). The rFF of normal marrow was measured in the pelvis of patients without diffuse pelvic disease (n = 88).

Statistical analysis

We compared the median of the mean rFF of bone disease between lesions arising from prostate cancer, breast cancer and myeloma, and, also, with normal marrow using Mann–Whitney U test, which was conducted with Bonferroni corrections for multiple comparisons where appropriate. Interobserver agreement was assessed by interclass correlation coefficient (ICC). Statistically significant differences were defined as $p < 0.05$, except for post-hoc tests, for which $p < 0.017$ (=0.05/3) was considered significant. All statistical analyses were performed with MedCalc (v. 12.1.0 for Microsoft Windows 2000/XP/Vista/7; MedCalc Software) and IBM SPSS Statistics for Apple Mac, v. 28 (IBM Corp.).

RESULTS

Patient demographics

Initially, 1304 patients with histologically proven metastatic prostate cancer, breast cancer or myeloma who underwent WB-MRI were identified; 1195 were excluded because patients were not treatment naïve or did not show recent disease progression prompting a change in therapy (n = 1137). In addition, patients were excluded due to poor image quality for analysis (n = 58). Hence, the remaining 110 patients comprised our final study population.

71 males and 39 females (median age = 66, range = 34–87 years) were enrolled. The majority (n = 52, 47.3%) had prostate cancer; 32 patients (29.1%) had myeloma and 26 (23.6%) had breast cancer. Patient demographic and tumour characteristics of the final included cohort is summarised in Table 2.

Comparing rFF of malignant bone disease

There was no significant difference in the median rFF of malignant bone lesions from breast cancer (14.46%), myeloma (13.12%) and prostate cancer (13.67%) ($p > 0.017$, Bonferroni correction) (Figure 3).

We also found that there was no significant difference in the median rFF of bone disease according to their anatomical locations ($p > 0.008$, Bonferroni correction) (Figure 4).

Comparing the rFF of malignant bone disease with normal marrow

Malignant bone lesions showed significantly lower median rFF (13.87%) compared with normal bone marrow (89.76%) with very little overlap ($p < 0.0001$) (Figure 5).

Interboserver agreement

The readers assessing WB-MRI showed excellent interobserver agreement for scoring across the whole skeleton (ICC = 0.95). WB-MRI also demonstrated excellent reliability across all other individual body regions with ICC estimates ranging from 0.94 to 0.96, all with narrow 95% confidence intervals (Table 3, Figure 6).

Table 2. Patient demographic and tumour characteristics

Characteristics (N = 110)	Number	Percentage, %
Age (median)	66	
Range	34–87	
Sex (female/male)	39/71	
Tumours		
Prostate	52	47.3
Breast	26	23.6
Myeloma	32	29.1

Figure 3. The boxplot shows the rFF of malignant bone lesions for each of the three malignancy groups. rFF, relative fat fraction.

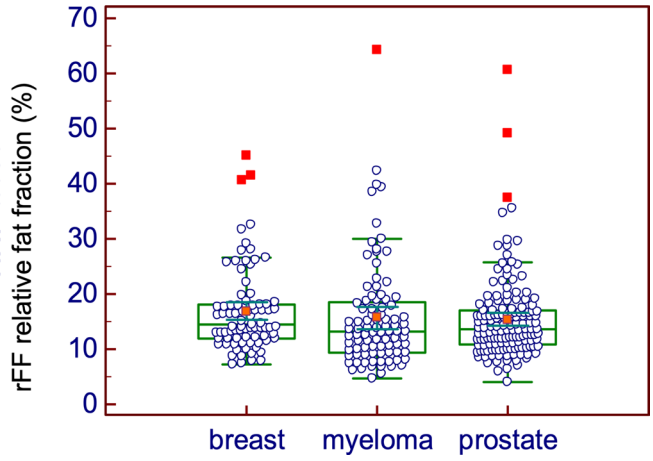

DISCUSSION

WB-MRI is increasingly used for the initial evaluation of bone disease in patients with different malignancies. Furthermore, in the past years, qualitative and quantitative assessments of WB-MRI have yielded promising results for monitoring treatment response[8–11] (Figure 7).

MR techniques have emerged as reliable tools for the non-invasive estimation of fat content, particularly in the liver, muscle and bone marrow.[12,13] Chemical shift MRI (in-phase and out-of-phase imaging) could be helpful in differentiating between lesions containing microscopic fat, with some studies suggesting that a signal drop of <20% at out-of-phase imaging compared to the in-phase imaging is more likely to represent a marrow-replacing neoplasm rather than a benign lesion.[14,15] However, this system shows limitations if used quantitatively, since measured values could be inaccurate or biased by fat-water ambiguity.[16,17]

Figure 4. The boxplot shows the rFF of malignant bone lesions divided by their anatomical location. rFF, relative fat fraction.

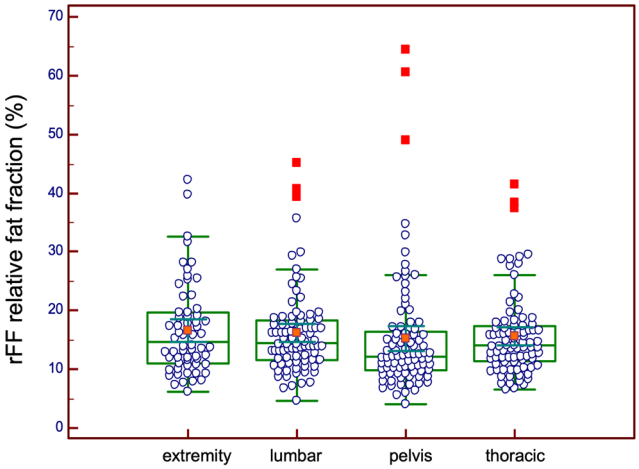

Figure 5. The boxplot shows the rFF of malignant bone lesions compared with normal bone marrow ($p < 0.0001$). Malignant bone lesions had low fat fraction, whereas normal bone marrow had a much higher fat fraction. rFF, relative fat fraction.

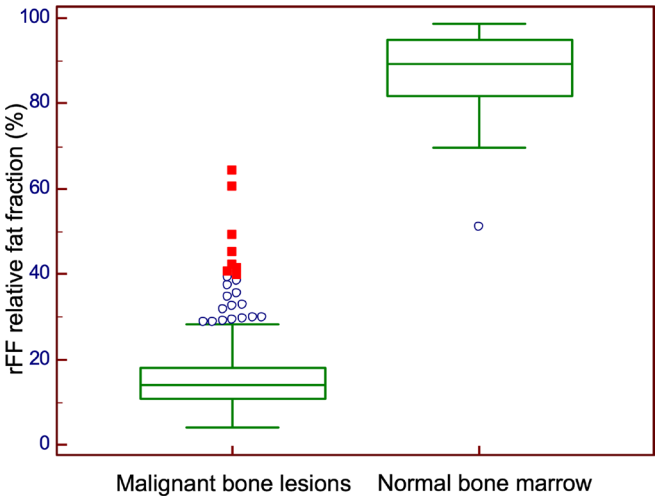

In our study, we used a two-point echo Dixon volumetric interpolated breath-hold examination technique, which enables fat quantification through the mapping of fat and water percentages. Accurate tissue fat quantification is confounded by T2* signal decay, field inhomogeneities, the spectral complexity of the fat molecules and T1 effects. In our study, the T1 weighting used for our Dixon acquisition still introduces a bias on FF estimates, and hence our fat fraction estimates are relative rather than absolute. Proton density fat fraction (PDFF) is a quantitative imaging biomarker of fat content which uses a low flip angle to minimise T1 bias and applies fat spectral modelling to account for the multipeak nature of fat[18,19]; however, this would require the acquisition of additional sequences with poor soft tissue contrast for qualitative disease assessment, which can prolong the overall duration of the WB-MRI. T_1W Dixon has the advantage of enabling the acquisition of quick T_1W anatomical images alongside fat and water images, thus removing the requirement for additional sequences, although at the expense of less accurate FF estimates. Due to the large difference in the rFF of bone disease compared with normal bone marrow, this pragmatic approach can be considered.

Although the Dixon technique has been applied to evaluate bone marrow fat composition, specifically focal bone lesions,[20] osteoporosis,[21] bone growth and development in children,[22] to our knowledge, this is the first application of a T_1 weighted implementation of the technique to compare the rFF of active bone lesions arising from breast, prostate and myeloma malignancies and the normal bone marrow, as well as their anatomical locations; and also to determine the inter-reader agreement.

Our study has shown that the rFF values in active bone lesion in three different malignancies are significantly lower than normal bone marrow, indicating the potential for rFF to enhance disease detection and potentially quantify the transition from active disease to remission and vice versa. Furthermore, no statistically significant differences in rFF values were found between

Table 3. Interobserver agreement as demonstrated by ICC for scoring WB-MRI for individual body regions and the whole skeleton

WB-MRI	ICC between observers (95% confidence interval)
Cervicothoracic spine	0.98 (0.96–0.98)
Lumbosacral spine	0.95 (0.92–0.97)
Pelvis	0.95 (0.92–0.97)
Extremity	0.93 (0.89–0.97)
Whole skeleton	0.95 (0.94–0.96)

ICC, intraclass correlation coefficient; WB-MRI, whole-body MRI.

Figure 6. Interobserver agreement as demonstrated by ICC for scoring WB-MRI for individual body regions. CI, confidence interval; ICC, intraclass correlation coefficient; WB-MRI, whole-body MRI.

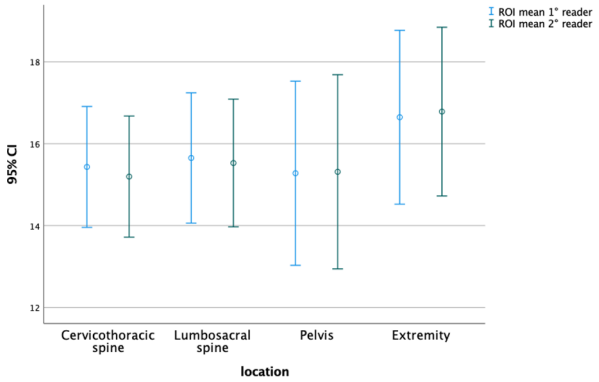

different tumour types and between different anatomical location, indicating the generalisability of these findings.

Our findings on the inter-reader agreement of rFF measured on WB-MRI confirm previous reports in MM,[23] of lumbar spine,[24] of liver[25] and subcutaneous adipose tissue.[26] The measurements of rFF in bone lesions have excellent reliability across the whole skeleton and in all individual body regions.

Few studies have investigated rFF quantification of bone marrow. Yoo et al[20] studied whether T_1 weighted FF maps using a modified Dixon sequence could help differentiate benign from malignant bone lesions in 120 patients subdivided in control, benign and malignant group. They found that the FF was the best associated variable to differentiate malignant from benign lesions, if compared with T_1W signal intensity (SI), T_1W SI of normal disc and lesion-to-disc ratio. However, this study was performed only on 3 T systems and in a split cohort of patients. Moreover, they did not compare the differences between the rFF according to the tumour types or anatomical location.

Takasu et al[7] demonstrated a significant decrease in lumbar spine T_1 weighted fat fraction in myeloma patients, compared with healthy volunteers, using iterative decomposition of water and fat with echo asymmetric and least-squares estimation MRI. In their cohort, discriminant analysis of FF showed that 92% of patients were classified correctly into symptomatic or non-symptomatic MM groups based on FF alone.

There are limitations to our study. First, our study is retrospective in patients with established metastatic bone disease. However, it is likely that our findings can be applicable to patients with early metastatic disease that require imaging for detection and follow-up. Second, although care was taken to draw the ROIs to encompass each lesion, the study results could be influenced

Figure 7. A 58-year-old male with multiple myeloma. The background marrow appears hypercellular which is characterise by diffuse high b900 and low ADC marrow signal (a, b). rFF can detect the focal active disease in the T8 (arrow in c). The detection of a focal active lesion fulfils the criteria for a high-risk bio-marker requiring therapy. ADC, apparent diffusion coefficient; rFF, relative fat fraction.

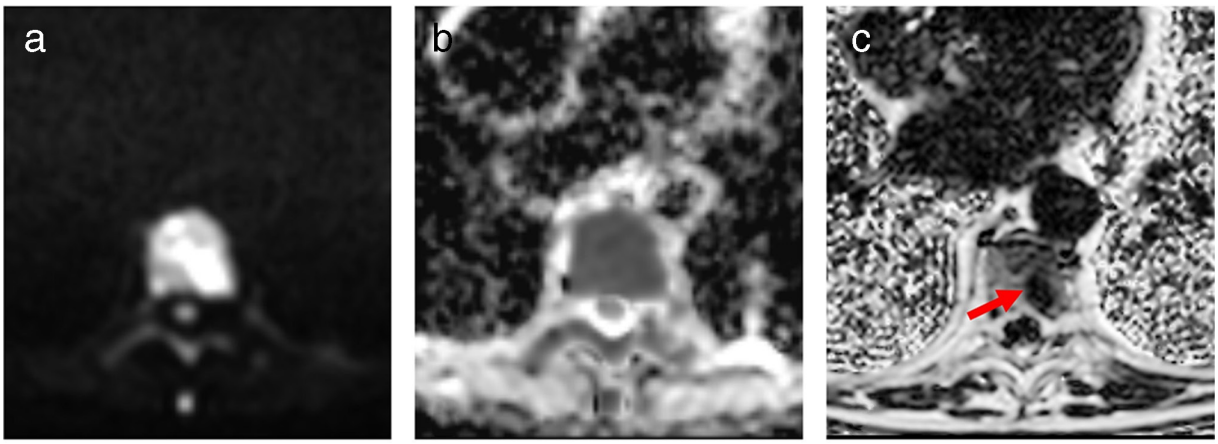

by the readers' decisions where the outer margin of the lesion was and the signal intensity threshold adopted. Nonetheless, this did not seem to affect the interobserver agreement of the rFF measurements. Thirdly, ROIs of normal bone marrow were evaluated only in the pelvis for patients without diffuse bone disease, without distinguishing between different imaging stations. Finally, this study did not control for age, menopausal status and previous treatment regimen; the former two factors may have a bearing on the rFF of normal marrow. Nonetheless, our study was conducted across an age range in the adult population (median 66 years), which is reflective of the ages when these malignant conditions would be encountered.Further research should be performed in the future to validate the clinical importance and relationship between quantitative assessment of lesions on rFF maps and their potential relationship to disease prognosis in breast, prostate and myeloma malignancies. In addition, as we did not corroborate our MRI study with contemporaneous CT findings, future studies may also be undertaken to understand to what extent the Dixon-derived rFF may be affected by the extent of bone sclerosis.

In summary, the rFF of malignant bone lesions from breast cancer, prostate cancer and myeloma obtained using a gradient-echo Dixon sequence was significantly lower than in normal bone marrow. Furthermore, the rFF has excellent inter-reader agreement, which could be useful for assessing the treatment response of bone metastases.

ACKNOWLEDGMENT

This study represents independent research supported by the National Institute for Health Research (NIHR) Biomedical Research Centre and the Clinical Research Facilities (CRF) at the Royal Marsden NHS Foundation Trust and the Institute of Cancer Research. The views expressed are those of the authors and not necessarily those of the NIHR or the Department of Health and Social Care.

REFERENCES

1. Carlin BI, Andriole GL. The natural history, skeletal complications, and management of bone metastases in patients with prostate carcinoma. *Cancer* 2000; **88**: 2989–94. https://doi.org/10.1002/1097-0142(20000615)88:12+<2989::aid-cncr14>3.3.co;2-h
2. Coleman RE. Clinical features of metastatic bone disease and risk of skeletal morbidity. *Clin Cancer Res* 2006; **12**: 6243s–62449. https://doi.org/10.1158/1078-0432.CCR-06-0931
3. Messiou C, Hillengass J, Delorme S, Lecouvet FE, Moulopoulos LA, Collins DJ, et al. Guidelines for acquisition, interpretation, and reporting of whole-body MRI in myeloma: myeloma response assessment and diagnosis system (MY-RADS). *Radiology* 2019; **291**: 5–13. https://doi.org/10.1148/radiol.2019181949
4. Padhani AR, Lecouvet FE, Tunariu N, Koh D-M, De Keyzer F, Collins DJ, et al. Metastasis reporting and data system for prostate cancer: practical guidelines for acquisition, interpretation, and reporting of whole-body magnetic resonance imaging-based evaluations of multiorgan involvement in advanced prostate cancer. *Eur Urol* 2017; **71**: 81–92. https://doi.org/10.1016/j.eururo.2016.05.033
5. Messiou C, Giles S, Collins DJ, West S, Davies FE, Morgan GJ, et al. Assessing response of myeloma bone disease with diffusion-weighted MRI. *Br J Radiol* 2012; **85**: e1198–203. https://doi.org/10.1259/bjr/52759767
6. Bray TJP, Singh S, Latifoltojar A, Rajesparan K, Rahman F, Narayanan P, et al. Diagnostic utility of whole body dixon MRI in multiple myeloma: A multi-reader study. *PLoS One* 2017; **12**: e0180562. https://doi.org/10.1371/journal.pone.0180562
7. Takasu M, Kaichi Y, Tani C, Date S, Akiyama Y, Kuroda Y, et al. Iterative decomposition of water and fat with echo asymmetry and least-squares estimation (IDEAL) magnetic resonance imaging as a biomarker for symptomatic multiple myeloma. *PLoS One* 2015; **10**(2): e0116842. https://doi.org/10.1371/journal.pone.0116842
8. Hillengass J, Ayyaz S, Kilk K, Weber M-A, Hielscher T, Shah R, et al. Changes in magnetic resonance imaging before and after autologous stem cell transplantation correlate with response and survival in multiple myeloma. *Haematologica* 2012; **97**: 1757–60. https://doi.org/10.3324/haematol.2012.065359
9. Chantry A, Kazmi M, Barrington S, Goh V, Mulholland N, Streetly M, et al. Guidelines for the use of imaging in the management of patients with myeloma. *Br J Haematol* 2017; **178**: 380–93. https://doi.org/10.1111/bjh.14827
10. Petralia G, Padhani AR. Whole-body magnetic resonance imaging in oncology: uses and indications. *Magn Reson Imaging Clin N Am* 2018; **26**: 495–507. https://doi.org/10.1016/j.mric.2018.06.003
11. Koutoulidis V, Terpos E, Papanikolaou N, Fontara S, Seimenis I, Gavriatopoulou M, et al. Comparison of MRI features of fat fraction and ADC for early treatment response assessment in participants with multiple myeloma. *Radiology* 2022; **304**: 137–44. https://doi.org/10.1148/radiol.211388
12. Gee CS, Nguyen JTK, Marquez CJ, Heunis J, Lai A, Wyatt C, et al. Validation of bone marrow fat auantification in the presence of trabecular bone using MRI. *J Magn Reson Imaging* 2015; **42**: 539–44. https://doi.org/10.1002/jmri.24795
13. Grimm A, Meyer H, Nickel MD, Nittka M, Raithel E, Chaudry O, et al. Evaluation of 2-point, 3-point, and 6-point Dixon magnetic resonance imaging with flexible echo timing for muscle fat Quantification. *Eur J Radiol* 2018; **103**: 57–64. https://doi.org/10.1016/j.ejrad.2018.04.011
14. Zampa V, Cosottini M, Michelassi C, Ortori S, Bruschini L, Bartolozzi C. Value of opposed-phase gradient-echo technique in distinguishing between benign and malignant vertebral lesions. *Eur Radiol* 2002; **12**: 1811–18. https://doi.org/10.1007/s00330-001-1229-6
15. Costa FM, Canella C, Vieira FG, Vianna EM, Meohas W, Marchiori E. The usefulness of chemical-shift magnetic resonance imaging for the evaluation of osteoid Osteoma. *Radiol Bras* 2018; **51**: 156–61. https://doi.org/10.1590/0100-3984.2017.0037
16. Eggers H, Börnert P. Chemical shift encoding-based water-fat separation methods. *J Magn Reson Imaging* 2014; **40**: 251–68. https://doi.org/10.1002/jmri.24568
17. Bray TJ, Chouhan MD, Punwani S, Bainbridge A, Hall-Craggs MA. Fat fraction mapping using magnetic resonance imaging:

insight into pathophysiology. *Br J Radiol* 2018; **91**: 20170344. https://doi.org/10.1259/bjr.20170344

18. Bydder M, Yokoo T, Hamilton G, Middleton MS, Chavez AD, Schwimmer JB, et al. Relaxation effects in the quantification of fat using gradient echo imaging. *Magn Reson Imaging* 2008; **26**: 347–59. https://doi.org/10.1016/j.mri.2007.08.012
19. Hamilton G, Yokoo T, Bydder M, Cruite I, Schroeder ME, Sirlin CB, et al. In vivo characterization of the liver fat ^{1}H MR spectrum. *NMR Biomed* 2011; **24**: 784–90. https://doi.org/10.1002/nbm.1622
20. Yoo HJ, Hong SH, Kim DH, Choi J-Y, Chae HD, Jeong BM, et al. Measurement of fat content in vertebral marrow using a modified dixon sequence to differentiate benign from malignant processes. *J Magn Reson Imaging* 2017; **45**: 1534–44. https://doi.org/10.1002/jmri.25496
21. Kühn J-P, Hernando D, Meffert PJ, Reeder S, Hosten N, Laqua R, et al. Proton-density fat fraction and simultaneous R2* estimation as an MRI tool for assessment of osteoporosis. *Eur Radiol* 2013; **23**: 3432–39. https://doi.org/10.1007/s00330-013-2950-7
22. Zhang C, Slade JM, Miller F, Modlesky CM. Quantifying bone marrow fat using standard T1-weighted magnetic resonance images in children with typical development and in children with cerebral palsy. *Sci Rep* 2020; **10**(1): 4284. https://doi.org/10.1038/s41598-019-57030-5
23. Barwick T, Orton M, Koh DM, Kaiser M, Rockall A, Tunariu N, et al. Repeatability and reproducibility of apparent diffusion coefficient and fat fraction measurement of focal myeloma lesions on whole body magnetic resonance imaging. *Br J Radiol* 2021; **94**: 20200682. https://doi.org/10.1259/bjr.20200682
24. Maas M, Akkerman EM, Venema HW, Stoker J, Den Heeten GJ. Dixon quantitative chemical shift MRI for bone marrow evaluation in the lumbar spine: a reproducibility study in healthy volunteers. *J Comput Assist Tomogr* 2001; **25**: 691–97. https://doi.org/10.1097/00004728-200109000-00005
25. Hooker JC, Hamilton G, Park CC, Liao S, Wolfson T, Dehkordy SF, et al. Inter-reader agreement of magnetic resonance imaging proton density fat fraction and its longitudinal change in a clinical trial of adults with nonalcoholic steatohepatitis. *Abdom Radiol (NY)* 2019; **44**: 482–92. https://doi.org/10.1007/s00261-018-1745-3
26. Berglund J, Johansson L, Ahlström H, Kullberg J. Three-point dixon method enables whole-body water and fat imaging of obese subjects. *Magn Reson Med* 2010; **63**: 1659–68. https://doi.org/10.1002/mrm.22385